Polymer Journal (2025) 57:665–677
https://doi.org/10.1038/s41428-025-01020-0

ORIGINAL ARTICLE

Smectic liquid crystalline poly(ester imide)s with low dielectric dissipation factors for high-frequency applications

Hayato Maeda[1] · Yucheng Liang[1] · Ryohei Hosoya[1] · Rika Marui[1] · Erina Yoshida[1] · Yuqian Chen[1] · Kan Hatakeyama-Sato[1] · Yuta Nabae[1] · Shiori Nakagawa[1] · Junko Morikawa[1] · Masatoshi Tokita[1] · Ririka Sawada[1] · Shinji Ando[1] · Yoshihiro Hayashi[2,3] · Ryo Yoshida[2,3,4] · Hidemine Furuya[1] · Teruaki Hayakawa[1]

Received: 3 December 2024 / Revised: 24 December 2024 / Accepted: 26 December 2024 / Published online: 14 February 2025

Abstract

High-frequency electronic applications increasingly require polymer-based insulators with low dielectric constants (D_k) and dissipation factors (D_f). Reducing molecular mobility effectively decreases the D_f of polyimides (PIs), which are widely used as interlayer dielectrics in semiconductor integrated circuits. In this study, we reduced molecular mobility by synthesizing smectic liquid crystalline polyimides (LC-PIs) via the use of diamines with phenyl benzoate structures and alkyl chains, and promoting mesogen stacking in LC structures. Self-supporting films were fabricated, and their dielectric properties were evaluated, revealing significantly lower D_f values than those of conventional PI. The functional groups responsible for increasing D_f are visualized via molecular dynamics simulations performed by applying a virtual alternating electric field to 3D models of the LC-PIs whose structure was confirmed via wide-angle X-ray diffraction. This study highlights the potential of smectic LC-PIs in the molecular design of polymeric materials with lower D_f.

Introduction

The demand for functional materials to support high-frequency communication technologies has accelerated with the growth of big data, artificial intelligence, and the Internet of Things. Devices for these applications are expected to promote faster speeds, higher capacity, low latency, and energy efficiency; thus, interlayer dielectric polymer materials with a low dielectric constant (D_k) and low dissipation factor (D_f) are essential for minimizing signal transmission losses [1–5]. Polyimides (PIs) are commonly used as interlayer dielectric materials owing to their excellent thermal stability, mechanical strength, and chemical resistance [3, 6, 7]. Substantial research efforts have been directed at further reducing both the D_k and D_f of dielectric materials in response to the demands of high-frequency applications [6, 8–17]. Dielectric loss is proportional to the product of frequency, the square root of D_k, and D_f; thus, reducing D_f is more important than decreasing D_k to minimize dielectric loss in high-frequency applications.

Various molecular design strategies, which are typically based on theoretical models such as the Debye equation and the Clausius–Mossotti relation, have been developed to achieve lower D_k values [18, 19]. These theories suggest that reducing the molecular polarizability and increasing the molar volume effectively reduce D_k. Experiments involving the incorporation of fluorine atoms [20–23], alicyclic structures [24–26], bulky structures [20, 21, 27], and cage-like siloxane structures [28, 29] have yielded promising results.

These authors contributed equally: Hayato Maeda, Yucheng Liang.

Supplementary information The online version contains supplementary material available at https://doi.org/10.1038/s41428-025-01020-0.

✉ Hidemine Furuya
furuya@cap.mac.titech.ac.jp

✉ Teruaki Hayakawa
hayakawa.t.ac@m.titech.ac.jp

[1] School of Materials and Chemical Technology, Institute of Science Tokyo, Tokyo, Japan

[2] The Institute of Statistical Mathematics, Research Organization of Information and Systems, Tachikawa, Tokyo, Japan

[3] The Graduate University for Advanced Studies, SOKENDAI, Tachikawa, Tokyo, Japan

[4] National Institute for Materials Science, Tsukuba, Ibaraki, Japan

In contrast, molecular design strategies to effectively reduce D_f remain largely unknown. Reducing the number of polar functional groups or introducing fluorine atoms can effectively reduce D_f [11]; however, reducing the number of polar functional groups in PIs, which inherently contain numerous imide groups, is challenging, and the use of fluorine is increasingly discouraged owing to environmental concerns [30, 31]. Additionally, reducing the molecular mobility, which resonates at the signal frequency, within PIs is also known to reduce D_f [8, 10, 32]. For example, Yin et al. demonstrated that nematic liquid crystalline (LC) structures can be introduced into PIs composed of 1,4-phenylene bis(1,3-dioxo-1,3-dihydroisobenzofuran-5-carboxylate) (TAHQ) and 2,2′-bis(-trifluoromethyl)benzidine (TEMB) by adjusting the solvent evaporation time during the formation of poly(amic acid) (PAA) films [10]. These structures can suppress the vibration of polar groups via molecular stacking, resulting in remarkably low D_f values. These findings suggest that LC-PIs are a promising new approach for achieving a lower D_f in dielectric materials. Compared with the nematic LC structure, the smectic LC structure with a layered arrangement restricts the motion of mesogens along their long axes, resulting in a reduction in molecular mobility. This layered arrangement, a unique structural characteristic of the smectic phase, increases its potential to decrease the D_f further. However, processing smectic LC-PIs into films suitable for evaluating their dielectric properties is still a challenging task because their molecular chains exhibit limited entanglement. As a result, the dielectric properties of smectic LC-PIs remain largely unexplored, which limits their application in high-frequency electronic materials.

In this study, we synthesized four types of PIs consisting of rigid phenyl benzoate-based structures with imide linkages and flexible alkyl chains of various lengths. Self-supporting films were fabricated and confirmed to exhibit smectic LC structures via wide-angle X-ray diffraction (WAXD) measurements. The D_f values of these films (approximately 0.003) were significantly lower than those of a conventional fully aromatic PI: pyromellitic dianhydride/4,4′-oxydianiline (PMDA/ODA). Molecular dynamics (MD) simulations were performed by applying a virtual alternating electric field to 3D models of the LC-PI structures, which were determined from their WAXD profiles. These simulations enabled visualization of the periodic torsional motion induced by the electric field for various functional groups in the polymer chains, demonstrating their contribution to the increase in D_f. These findings provide valuable insights that will facilitate the molecular design and development of PIs with lower dielectric loss and highlight the potential of smectic LC structures in reducing D_f.

Materials and methods

Materials

Unless otherwise specified, commercial reagents and solvents were used as received without further purification. Methyl 4-hydroxybenzoate, 1,6-dibromohexane, 1,12-dibromododecane, thionyl chloride ($SOCl_2$), 4-nitrophenol, and 10% palladium on carbon (Pd/C, wetted with ca. 55% water) were purchased from Tokyo Chemical Industry Co., Ltd. (TCI). 3,3′,4,4′-Biphenyltetracarboxylic dianhydride (BPDA), 1,4-phenylene bis(1,3-dioxo-1,3-dihydroisobenzofuran-5-carboxylate) (TAHQ) and pyromellitic dianhydride (PMDA) were purchased from TCI and recrystallized from acetic anhydride before use. 4,4′-Oxydianiline (ODA) was purchased from TCI and recrystallized from ethanol before use. *N*,*N*-Dimethylformamide (super dehydrated) (DMF), *N*-methyl-2-pyrrolidone (super dehydrated) (NMP), potassium carbonate (K_2CO_3), potassium hydroxide (KOH), and hydrochloric acid (HCl) were obtained from FUJIFILM Wako Pure Chemical Industries, Ltd. Pyridine was purchased from Sigma–Aldrich. Ethanol (EtOH), methanol, *n*-hexane, dichloromethane (DCM), and 1,2-dichloroethane (DCE) were purchased from KANTO Chemical Co., Inc.

Instrumentation

^1H and ^{13}C nuclear magnetic resonance (NMR) spectra were recorded via a JEOL JNM-ECS400 (400 MHz) spectrometer with deuterated chloroform ($CDCl_3$) and deuterated dimethyl sulfoxide (DMSO-d_6). Fourier transform infrared spectroscopy (FT-IR) was conducted using a JASCO FT/IR-4100 spectrometer. The LC structures were observed via an Olympus BX51 polarized optical microscope (POM) equipped with an optical polarizer and a temperature control system (Mettler Toledo FP90/FP82HT). The inherent viscosities (η_{inh}) of PAAs with a solid content of 0.5 g/dL were measured in NMP at 30 °C via an Ostwald viscometer. Thermogravimetric analysis (TGA) was performed at a heating rate of 10 °C/min via an SII EXSTAR TG/DTA7300 thermal analyzer. Differential scanning calorimetry (DSC) measurements were conducted via an SII EXSTAR DSC7020 instrument under a nitrogen gas atmosphere at a temperature scan rate of 10 °C/min. Ultrafast scanning calorimetry (FSC) was performed under nitrogen gas at temperature scan rates of 2000, 5000, and 10,000 °C/s in accordance with an established procedure [33]. Wide-angle X-ray diffraction (WAXD) measurements were performed at the BL40B2 beamline of SPring-8 with a wavelength of 1.00 Å and a sample-to-detector distance of 108 mm. D_k and D_f were measured in transverse electric (TE_{011}) mode at frequencies of 10 GHz and 20 GHz via a cavity resonator (AET, Japan) connected to a vector

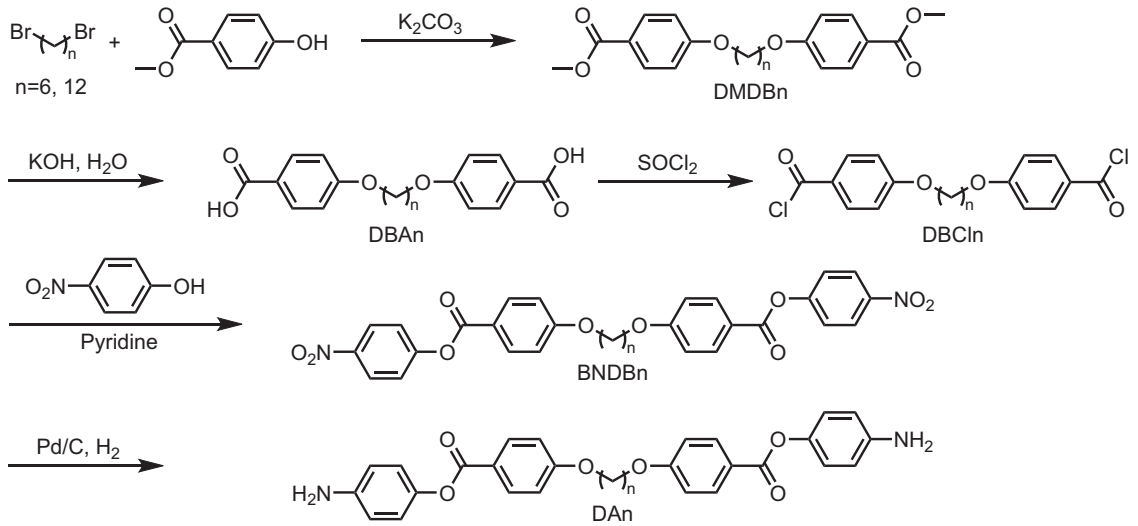

Scheme 1 Synthesis of diamines with phenyl benzoate structures and alkyl chains

network analyzer (Anritsu MS46122B, Japan). The temperature and relative humidity of the measurement environment were maintained at 22 °C and 30% RH, respectively.

Monomer synthesis

Two types of diamine monomers with phenyl benzoate structures and alkyl chains were synthesized via a five-step procedure (Scheme 1). The synthesized diamines are denoted "DAn", where n is the number of carbon atoms in the alkyl chain.

DMDBn

The synthesis of DMDB6 is described as a representative example. K_2CO_3 (300 mmol, 41.46 g) and methyl 4-hydroxybenzoate (240 mmol, 36.52 g) were added to DMF (250 ml) and stirred for 1 h at room temperature. 1,6-dibromohexane (100 mmol, 15.38 ml) was then added, and the reaction mixture was stirred overnight at 80 °C. The solution was cooled to room temperature and reprecipitated with water followed by EtOH. The precipitate was collected by filtration, and dried under reduced pressure at 70 °C overnight, yielding a white powder (36.72 g, 95%).

DBAn

The synthesis of DMA6 is described as a representative example. DMDB6 (50 mmol, 19.32 g) was added to a mixture of deionized water (40 ml) and EtOH (250 ml). KOH (240 mmol, 13.47 g) was then added, and the mixture was stirred under reflux overnight at 90 °C. Subsequently, 2 M HCl (aq) was added dropwise until the mixture became acidic, as confirmed by pH test paper, and the solution was stirred for 2 h at room temperature. The resulting mixture was filtered, and the solid was reprecipitated with EtOH. The precipitate was collected by filtration and dried under reduced pressure at 70 °C overnight, yielding a white powder (17.26 g, 94%).

DBCln

The synthesis of DBCl6 is described as a representative example. DBA6 (70 mmol, 25.79 g) was added to $SOCl_2$ (110 ml). The mixture was stirred under reflux at 90 °C for 3 h under nitrogen. The resulting solution was evaporated under reduced pressure, and the residue was washed with *n*-hexane. The product was dried at 40 °C overnight under reduced pressure and recrystallized from a *n*-hexane–toluene mixture, yielding a white powder (27.26 g, 98%).

BNDBn

The synthesis of BNDB6 is described as a representative example. 4-Nitrophenol (64 mmol, 8.90 g) and pyridine (24 ml) were added to a two-neck flask under a nitrogen atmosphere and stirred in an ice bath for 1 h. In a separate flask, DBCl6 (16 mmol, 6.32 g) was dissolved in pyridine (35 ml) and then added slowly to the 4-nitrophenol solution at 0 °C. The reaction mixture was stirred overnight at 70 °C under a nitrogen atmosphere before being precipitated in EtOH. The resulting solid was collected by filtration and dried under reduced pressure overnight at 60 °C. The crude product was purified by silica gel chromatography using DCM as the eluent, followed by rotary evaporation. The purified solid was dried under reduced pressure overnight at 40 °C, yielding a white solid (7.30 g, 76%).

Table 1 Component monomer combinations and experimentally measured properties of the polyimide samples

Label	Tetracarboxylic Dianhydride	Diamine	η_{inh}[a] [dL/g]	$T_{d5\%}$ [°C]	Experimental D_k		Experimental D_f	
					10 GHz	20 GHz	10 GHz	20 GHz
PI-B6	BPDA	DA6	0.89	459	3.34	3.28	0.0037	0.0034
PI-B12	BPDA	DA12	0.85	440	3.21	3.01	0.0041	0.0033
PI-T6	TAHQ	DA6	1.13	434	3.10	3.17	0.0038	0.0035
PI-T12	TAHQ	DA12	1.14	431	2.96	3.06	0.0046	0.0039
PMDA-ODA	PMDA	ODA	1.25	566	3.31	3.30	0.0104	0.0110

[a]The inherent viscosities (η_{inh}) of the PAAs were measured in NMP at a solid content of 0.5 g/dL at 30 °C via an Ostwald viscometer

DAn

The synthesis of DA6 is described as a representative example. BNDB6 (12 mmol, 7.21 g) was added to DMF (160 ml) and stirred at 65 °C until fully dissolved. EtOH (32 ml) was then added slowly to prevent precipitation. Pd/C (240 mg) was then added, and the system was sequentially purged with nitrogen followed by hydrogen. The mixture was stirred overnight at 65 °C, after which the solution was filtered through Celite, and the filtrate was precipitated with EtOH. The precipitate was collected by filtration, and dried under reduced pressure overnight at 120 °C. The solid obtained was recrystallized from DCE, yielding a pink solid (5.48 g, 85%).

Synthesis of poly(amic acid)s

Various PAAs were synthesized as precursors of PIs by the polymerization of the corresponding source materials (Table 1). A representative procedure using DA6 and BPDA is provided as an example. In a two-neck flask, DA6 (1 mmol, 0.541 g) was dissolved in NMP under a nitrogen atmosphere at room temperature. Subsequently, BPDA (1 mmol, 0.294 g) and additional NMP were added to the solution, and the mixture was stirred for 24 h under an argon atmosphere, maintaining the monomer concentration at 15–20 wt.%. The solution was subsequently diluted with NMP until it could be aspirated into a pipette. The solution was reprecipitated in methanol, and the precipitate was collected by filtration, and dried under reduced pressure overnight at 50 °C.

Fabrication of polyimide films

To fabricate the PI films, the PAA solutions were cast onto glass substrates (10 cm × 10 cm) and spread evenly with a glass rod. The films were heated at 80 °C for 30 min, followed by heating at 250 °C for 3 h under reduced pressure. The PI films were detached from the glass substrates by immersion in water until separation. Five types of PAA and corresponding PI films were prepared from the diamines and dianhydrides listed in Fig. 1, including one control sample.

The chemical structures of the PIs were determined based on their constituent tetracarboxylic dianhydride and diamine, following the format PI-(first letter of the dianhydride abbreviation) (number of carbons in the alkyl chain). For example, PI-B6 denotes a PI comprising the BPDA and DA6. Additionally, a control PI was synthesized from PMDA and ODA, denoted as PMDA/ODA.

Molecular dynamics simulations

Molecular dynamics (MD) simulations were conducted via the large-scale atomic/molecular massively parallel simulator (LAMMPS) [34] implemented in RadonPy [35], an automated platform for physical property calculations through all-atom classical molecular dynamics simulations. For further details regarding the force field parameterization and simulation protocols, please refer to the original RadonPy publication [35].

The polymer chains were arranged manually within the simulation cell based on the smectic structure estimated from the results of WAXD measurements via Winmostar [36]. These chains were placed in the cell with periodic boundary conditions applied in all directions. The structure was equilibrated for 500 ps using a Nosé–Hoover thermostat at 300 K. The force field used for all the simulations was the improved general Amber force field version 2 (GAFF2_mod) [37].

After force field parameterization and equilibration, the alternating electric field was converted to a force vector that depends on the atomic charge via the *"fix efield command"* implemented in LAMMPS, and the resulting forces was applied to the atoms. These simulations were performed under an alternating electric field E at 10 GHz with the NVT ensemble. Since E is theoretically proportional to the polarization vector P, the strength of E was set at a point where this proportional relationship was maintained for each simulation system. Owing to the anisotropy of the

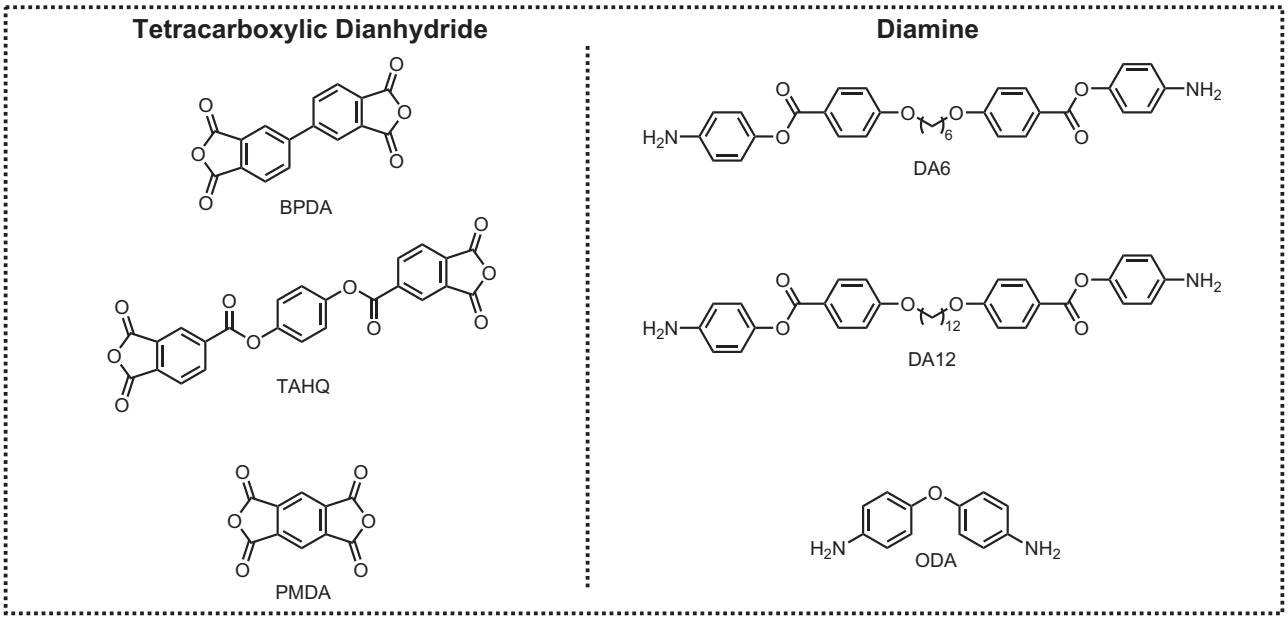

Fig. 1 Chemical structures of the monomers used to synthesize the polyimides

smectic structure, the electric field was applied in the X, Y, and Z directions, and the average values across these three directions were used to calculate D_f.

To calculate D_f, an external electric field $E = E_0 \cos(wt)$ was applied. The dipole moments p were used to compute the polarization $P = \frac{\sum_i p_i}{V}$, where V is the system volume. The electric displacement D was subsequently obtained as $D = \varepsilon_0 E + P$, where ε_0 is the permittivity of free space. The phase difference δ of the polarization relative to the electric field was calculated, and through complex analysis, the real part $\varepsilon' = D_k = \frac{D_0}{\varepsilon_0 E_0}\cos\delta + n^2$ and imaginary part $\varepsilon'' = \frac{D_0}{\varepsilon_0 E_0}\sin\delta$ of the dielectric constant were derived. n^2 in ε' is the square of the refractive index calculated with the Lorentz–Lorenz equation via the dipole polarizability obtained via density functional theory calculations [35] and is applied as a correction term assuming the contribution of the electronic polarization. The ratio of these components $\varepsilon''/\varepsilon'$ represents D_f.

The correlation between molecular motion and the dielectric response was explored via cross-correlation analysis with the alternating electric field and torsional motion within the polymer chains as variables. This analysis method is based on calculating the cross-correlation coefficient c_k^{norm} to capture the maximum correlation between the electric field and dihedral angle changes. The electric field $\boldsymbol{u} = \{x_1, x_2, x_3, \ldots\}$ and the dihedral angle $\boldsymbol{v} = \{y_1, y_2, y_3, \ldots\}$ are represented as time series data, and the cross-correlation function c_k and its normalized form c_k^{norm} are calculated as shown in Eqs. (1) and (2):

$$c_k = \sum_t \boldsymbol{u}_{t+k} \cdot \boldsymbol{v}_t = \sum_t (x_i - \overline{x})_{t+k} \cdot (y_i - \overline{y})_t \quad (1)$$

$$c_k^{norm} = \frac{\sum_t (x_i - \overline{x})_{t+k} \cdot (y_i - \overline{y})_t}{\sqrt{\sum (x_i - \overline{x})^2}\sqrt{\sum (y_i - \overline{y})^2}}, \quad (2)$$

where k is the time lag between $\boldsymbol{u}$ and $\boldsymbol{v}$. An absolute value of the maximum c_k^{norm} within one period of an electric field corresponds to the maximum correlation coefficient $C_{\max}$ between the electric field and a dihedral angle. Among the large number of dihedral angles in a model, specific dihedral angles with periodic motion induced by an electric field are identified by $C_{\max}$. Since the substructures containing these dihedral angles contribute largely to the deflection of the dipole moment, $C_{\max}$ can be regarded as a descriptor for investigating the structure–dielectric loss relationship.

Results and discussion

Synthesis of polyimides

Four types of PIs were synthesized with alternating rigid and flexible segments. The rigid segments contain mesogens based on phenyl benzoate or biphenyl units, whereas the flexible segments consist of aliphatic chains that act as spacers. These structures are typical of main-chain LC

polymers [38–42]. In addition to a control PMDA-ODA PI, four PIs were prepared by combining commercially available tetracarboxylic dianhydrides (TAHQ and BPDA) with two custom-synthesized diamines (DA6 and DA12), each featuring alkyl chains of different lengths.

The diamines DA6 and DA12, each containing two phenyl benzoate units linked by an alkyl chain, were synthesized via a five-step process involving Williamson ether synthesis, hydrolysis of the methyl ester, chlorination of the carboxylic acid, esterification, and reduction of the nitro group (Scheme 1). The chain length of each diamine was adjusted by using different dibromoalkanes as starting materials. According to reported patents [43], An intermediate, DBA6, can be synthesized in a single step from 1,6-dibromohexane and 4-hydroxybenzoic acid. However, additional protection and deprotection steps were introduced in this study to minimize side reactions. The final products, DA6 and DA12, were recrystallized from 1,2-dichloroethylene.

The PIs were synthesized via a two-step process using PAA as an intermediate. The inherent viscosities (η_{inh}) of the PAAs ranged from 0.85 to 1.25 dL/g (Table 1), which indicates efficient polymerization. PI films were obtained by thermal imidization of the corresponding PAAs. The completion of thermal imidization was confirmed by FT-IR spectroscopy (Fig. 2A) based on the appearance of the characteristic absorption bands at 1372 cm^{-1} (stretching of imide C–N bonds), 1722 cm^{-1} (asymmetric stretching of imide C=O bonds), and 1775 cm^{-1} (symmetric stretching of imide C=O bonds) and the absence of a peak at approximately 1661 cm^{-1} (amide −CO–NH– bonds). Figure 2B shows the appearance of four PI films obtained from the synthesized diamines. The films were flexible and self-supporting, with thicknesses ranging from 20 to 30 μm, which reveals a sufficiently high molecular weight and adequate chain entanglement, as indicated by the inherent viscosity of the PAAs (Table 1). The films were light brown, nearly transparent, with a slight whitish haze, which slightly varied among the samples.

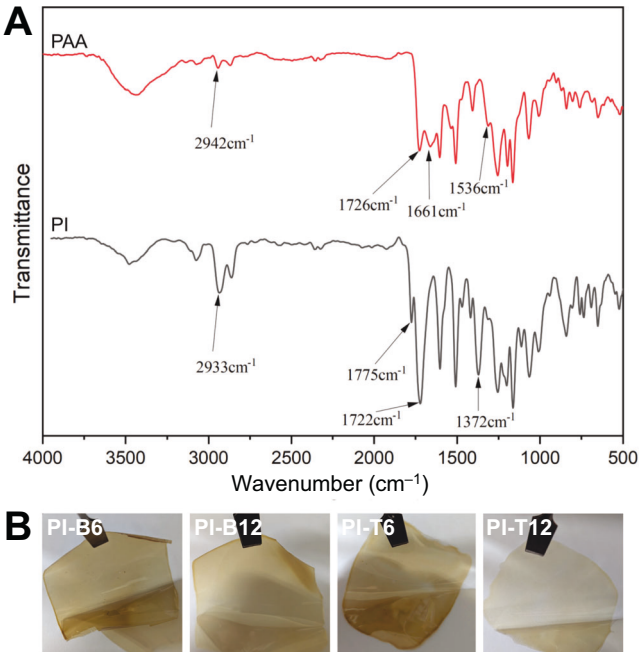

Fig. 2 **A** FT-IR spectra of polyimide (PI) and PAA, with PI-B6 as a representative. The FT-IR spectrum of the representative PAA (B6) exhibited characteristic peaks at 1726 cm^{-1} (carboxyl C=O) and 1661 cm^{-1} (amide C=O stretching), as well as a peak at 1536 cm^{-1} corresponding to amide C–N stretching. In the FT-IR spectrum of the prepared PI (B6), the peaks for the amic acid groups disappeared, and the characteristic imide peaks at 1775 cm^{-1} (imide C=O asymmetric stretching), 1722 cm^{-1} (imide C=O symmetric stretching), and 1372 cm^{-1} (imide C–N stretching) appeared, indicating complete imidization. **B** Appearance of the newly synthesized PI films

Higher-order structures of the LC-PIs

The higher-order structures of the synthesized PI films were investigated via WAXD. The spectra of the PI films showed distinct peaks in the q range below 8 nm^{-1} (Fig. 3B), which corresponds to the layer spacing typical of the smectic phase, with each sample showing structural differences. The WAXD profile of PI-B6 displayed a broad peak comprising two peaks with d-spacings of approximately 3.7 nm and 2.6 nm, whereas those of PI-B12, PI-T6, and PI-T12 each showed a single, sharp peak with respective d-spacings of 3.3 nm, 4.3 nm, and 4.7 nm. These findings indicate that each PI has distinct structural characteristics in its smectic layer arrangement. The d-spacing of approximately 3.7 nm in PI-B6 is similar to the length of the PI repeating unit calculated via an all-*trans* conformation model (Fig. 3C). In contrast, the 2.6 nm d-spacing in PI-B6, as well as the peaks in the patterns of PI-B12, PI-T6, and PI-T12, are shorter than the expected all-*trans* repeat unit lengths, which indicates variations in molecular conformation. Kricheldorf et al. [44] showed that main-chain-type LC-PIs can allow alkyl spacers to adopt gauche conformations to form smectic structures; thus, our findings imply that PI-B6 likely has a less complete smectic structure owing to the distribution of molecules with various alkyl chain conformations, which may affect layer stacking and ordering. In contrast, PI-B12, PI-T6, and PI-T12 contain domains with more uniform conformations, possibly featuring a predominance of alkyl chains in the *gauche* conformation (Fig. 3D).

Further analysis of the WAXD profile revealed additional peaks at approximately $q = 15$ nm^{-1}, which are attributed to the lateral packing of mesogens or polymer chains within a smectic layer. The number and sharpness of these peaks reflect the positional order of mesogens within a smectic layer, which reveals different structural arrangements depending on the PI

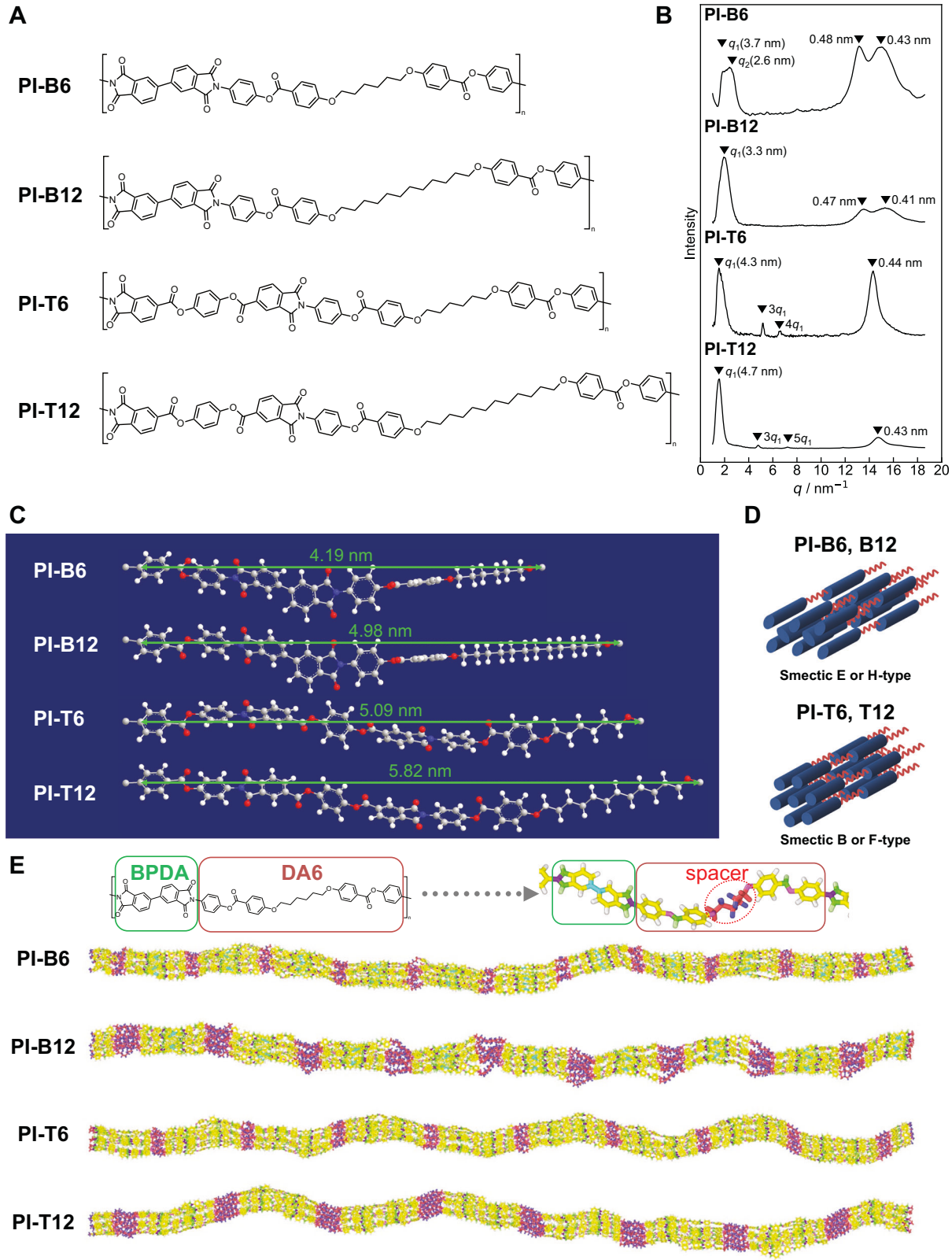

Fig. 3 **A** Chemical structures of the repeating units in the polyimides. **B** WAXD profiles of the PI films. **C** 3D model of the repeating unit in an all-trans conformation, showing the calculated periodic repeat length. **D** Proposed mesogen stacking arrangement inferred from the WAXD measurements. **E** 3D models of the LC-PIs based on the WAXD profiles. The bonds are color-coded by atom type, as shown in the top snapshot of the PI-B6 model

type. The existence of two peaks indicates that PI-B6 and PI-B12, comprising BPDA, pack mesogens into a centered rectangular lattice (or a pseudohexagonal lattice) rather than into hexagonal lattices such as those in smectic E or H (or K) structures. In contrast, PI-T6 and PI-T12, comprising TAHQ, likely form smectic B or F (or I) structures, characterized by a mesogen packed in a hexagonal lattice. The distinctions between smectic E and H structures, as well as between smectic B and F, lie in the orientation of the mesogens relative to the layer normal: in smectic E and B structures, mesogens arrange their long axes parallel to the layer normal, whereas, in smectic H and F structures, mesogens arrange their long axes in a direction tilted from the layer normal. A detailed determination of the mesogen tilt angle would require a 2D WAXD profile from an oriented sample. However, owing to the challenges in preparing an oriented sample, further investigation in this regard was not possible.

Based on the WAXD profiles, we constructed 3D models of the PIs, as shown in Fig. 3E, assuming smectic B or E arrangements with the mesogens aligned parallel to the layer normal. These models comprise smectic LC arrangements, where PI chains with gauche conformations in the alkyl segments show minimal undulation along the chain. The response of these 3D models to an applied alternating electric field is discussed in a subsequent section.

Thermal properties of the PI films

The effects of the molecular structure on the thermal stability, optical properties, and thermal behavior of the PI films were analyzed via TGA, POM under thermal conditions, DSC, and FSC.

TGA thermograms demonstrated the high thermal stability of the PIs, with a weight loss of only 5% observed at temperatures exceeding 400 °C (Table 1). This exceptional thermal stability was attributed to the presence of benzene rings and nitrogen-containing five-membered heterocycles in the PI backbone, which increase the resistance to thermal degradation. These results confirm the thermal resilience of the PI films and underscore their potential applicability in thermally demanding environments.

POM images of untreated PI films revealed no significant optical textures (Fig. 4A); however, distinct optical textures characteristic of LC materials appeared when the films were lightly rubbed with a stainless-steel spatula, likely because the rubbing process aligns the mesogens along the rubbing direction, resulting in anisotropic optical properties typical of LC polymers (Fig. 4B). This alignment creates ordered domains that interact with polarized light, producing the observed textures. To investigate the phase transition behavior of these samples, POM observations were conducted while the samples were heated to 350 °C. Remarkably, these textures showed minimal changes even after they were heated to 350 °C. Additionally, DSC measurements performed at a scanning rate of 10 °C/min over the temperature range from –30 °C to 350 °C detected no distinct endothermic or exothermic peaks, which indicates that phase transitions in the PIs could not be captured by either POM or DSC.

FSC measurements were conducted on untreated PI films at temperature scan rates of 2000, 5000, and 10,000 °C/s under a nitrogen atmosphere to investigate phase transitions that could not be observed by POM or DSC [33, 45]. The results for a scan rate of 10,000 °C/s are shown in Fig. 4C, whereas the data for 2000 and 5000 °C/s are provided in the Supplementary Information (Figs. S29 and S30). Endothermic and exothermic peaks were observed during heating and cooling, respectively, at temperatures above 250 °C. These peaks are presumed to originate from phase transitions within the PI structure. These findings indicate that the smectic LC phase formed at room temperature in the PI films remains stable even at temperatures exceeding 250 °C. FSC, capable of heating to approximately 600 °C, detected thermal events that are undetectable by POM or DSC, enabling the analysis of thermal behavior beyond the degradation temperature measured by TGA.

Dielectric properties measurement

The experimental values of the dielectric constant (D_k) and dielectric dissipation factor (D_f) of the four types of smectic LC-PI films and the PMDA/ODA control film measured at 10 and 20 GHz are presented in Table 1. The D_k values of the smectic LC-PIs are close to those of PMDA/ODA; however, their D_f values are significantly lower. These results indicate that the unique smectic structures of the LC-PIs significantly reduce D_f by restricting molecular mobility through the highly ordered stacking of mesogens. The difference in structural ordering is supported by WAXD measurements. For PMDA/ODA, a strong amorphous halo at $q \approx 13\ \mathrm{nm}^{-1}$ (Fig. S31) indicates its nearly amorphous structure. In contrast, the absence of such a halo in the smectic LC-PIs (Fig. 3B) confirms the highly ordered mesogen stacking characteristic of smectic LC structures.

The D_k values of the smectic LC-PIs ranged from 3.0 to 3.3 at both 10 and 20 GHz, close to or slightly lower than that of PMDA/ODA (3.3). The LC-PIs prepared in this study were not specifically designed to alter the molecular volume or polarizability, as described by the Clausius–Mossotti relation, which may explain the limited reduction in D_k. According to these theories, introducing less polar groups or incorporating bulkier structures in the PI chain can facilitate further reduction of D_k. Conversely, these PIs presented D_f values of 0.003–0.005 at both 10 and 20 GHz,

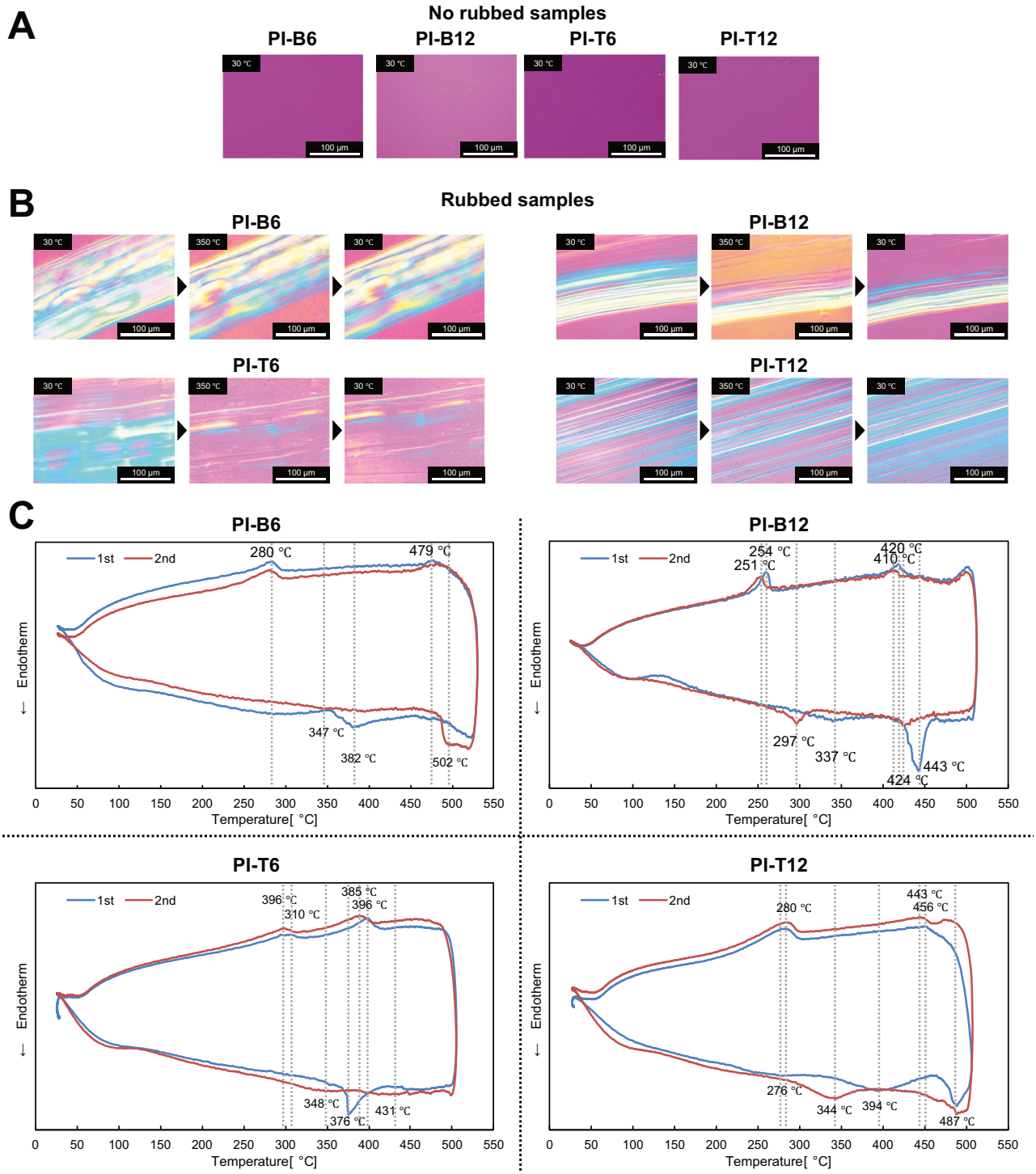

Fig. 4 POM observations and FSC measurements of the PI films. The POM images were acquired under a nitrogen atmosphere. **A** Untreated samples at 30 °C, **B** treated samples at 30 °C, 350 °C, and samples after cooling to 30 °C. **C** FSC results for a heating rate of 10,000 °C/s, showing the temperatures that correspond to the main endothermic and exothermic peaks

which are substantially lower than those of PMDA/ODA (0.010–0.011). This reduction in D_f is attributable to the mesogen stacking structure inherent to the smectic LC phase. The layered structure restricts molecular vibrational motion in a manner that is both perpendicular and parallel to the PI chains, effectively limiting their molecular mobility and significantly reducing D_f. These findings indicate that the formation of a smectic LC structure effectively reduces local molecular chain vibrations under an alternating electric field, thus reducing D_f.

Molecular dynamics simulation-based analysis of dielectric properties

MD simulations were performed by applying a virtual alternating electric field to 3D models of smectic LC-PIs, whose structures were determined based on WAXD profiles. Previous studies have shown that at frequencies of 1 GHz, 10 GHz, and 100 GHz, D_f is attributed primarily to the inability of orientational polarization—resulting from the reorientation or relaxation of dipoles—to keep pace with the alternating electric field [11, 13]. The D_f calculations yielded values in the range of approximately 0.001–0.002, which were in approximate agreement with the experimental results of 0.003–0.005. Recent studies suggest that the dielectric properties of PIs are significantly affected by the amount of adsorbed water under experimental conditions [13, 46, 47]; however, the MD simulations in this study did not account for the influence of adsorbed water. We are currently conducting further systematic analyses of D_f for PIs by comparing the MD simulations with the experimental values of 0% RH obtained by extrapolating the measurements at 10–60% RH [13], which reveals that the deviation observed in this study was influenced by water adsorption. A detailed report of these findings is being prepared.

For a more detailed understanding of which functional groups contribute to the increase in D_f, we evaluated the maximum cross-correlation coefficient C_{max} between the alternating electric field and all the dihedral angles in a model. Figure 5 shows snapshots that visualize C_{max} along the polymer chain. In this visualization, as the C_{max} values increase, the color transitions from black to white to yellow. Figure 5 presents the results for PI-B6, which was chosen as a representative example, at various frequencies (1, 10, and 100 GHz), with a virtual alternating electric field applied in the X, Y, and Z directions, with the X direction aligned with the molecular chain orientation. In Fig. 5A, we observe that when the electric field is applied in the direction of the molecular chain orientation, the positions of the functional groups showing a periodic torsional motion induced by the electric field in yellow remain consistent across different frequencies, which indicates no significant frequency dependence. This behavior reveals that, for smectic LC-PIs with aligned molecular chains, the dielectric performance may remain stable across a wide range of signal frequencies. This finding implies that when smectic LC-PIs are utilized, the molecular design of the PI dielectric material may not require modification, even as signal frequencies increase in future applications. Furthermore, Fig. 5B presents an enlarged portion of the 10 GHz results, with representative functional groups highlighted by colored rectangles. This panel shows that when the electric field is applied in the X direction, the imide groups appear in colors ranging from black to white, whereas they appear in shades from white to yellow when the field is applied in the Y and Z directions. Additionally, for the spacer segments composed of alkyl chains and ether groups, yellow is observed when the electric field is applied in the Y direction, whereas the region colored yellow is less noticeable when the field is applied in the X and Z directions. Conversely, the ester bonds are highlighted in yellow in all three field directions, which shows strong periodic motion irrespective of the direction of the electric field. A statistical summary of these findings at 10 GHz is presented in Fig. 5C. In Fig. 5C, all C_{max} in a model are classified by imide, ester, and spacer moieties and are represented as a probability density distribution. Figure 5C statistically supports the differences in the X, Y, and Z directions discussed above.

These findings align with the fact that oriented PI films exhibit anisotropy in their dielectric properties based on the alignment of their main chains [13, 48]. The MD simulations presented in Fig. 5 similarly reveal a correlation between molecular chain orientation and dielectric anisotropy, thereby further supporting the connection between structural alignment and dielectric performance. Furthermore, the minimal variation in the periodic motion of substructures between 1 GHz and 100 GHz indicates that the aligned smectic LC structure of the PI exhibits robust stability against a wide range of frequency variations; this stability highlights its potential as a reliable dielectric material for high-frequency signal transmission, which indicates that the design of smectic LC-PI dielectric materials may not require changes, even with increasing signal frequencies.

Conclusions

Four smectic LC-PIs containing phenyl benzoate structures and alkyl chains were successfully synthesized and processed into self-supporting films. These PIs are self-assembled into smectic LC structures, as confirmed by WAXD, POM, and FSC. The smectic LC-PIs presented significantly lower D_f values than conventional PI (PMDA/ODA), highlighting the effectiveness of smectic ordering in reducing dielectric loss. MD simulations further contributed to understanding the dielectric behavior of these materials. By applying a virtual alternating electric field to the 3D models based on WAXD profiles, the simulations enabled visualization of the periodic torsional motion induced by the electric field for various functional groups in the polymer chains, demonstrating the contribution of these functional groups to the increase in D_f. These results suggest that incorporating smectic LC structures provides not only a promising molecular design strategy to reduce D_f in

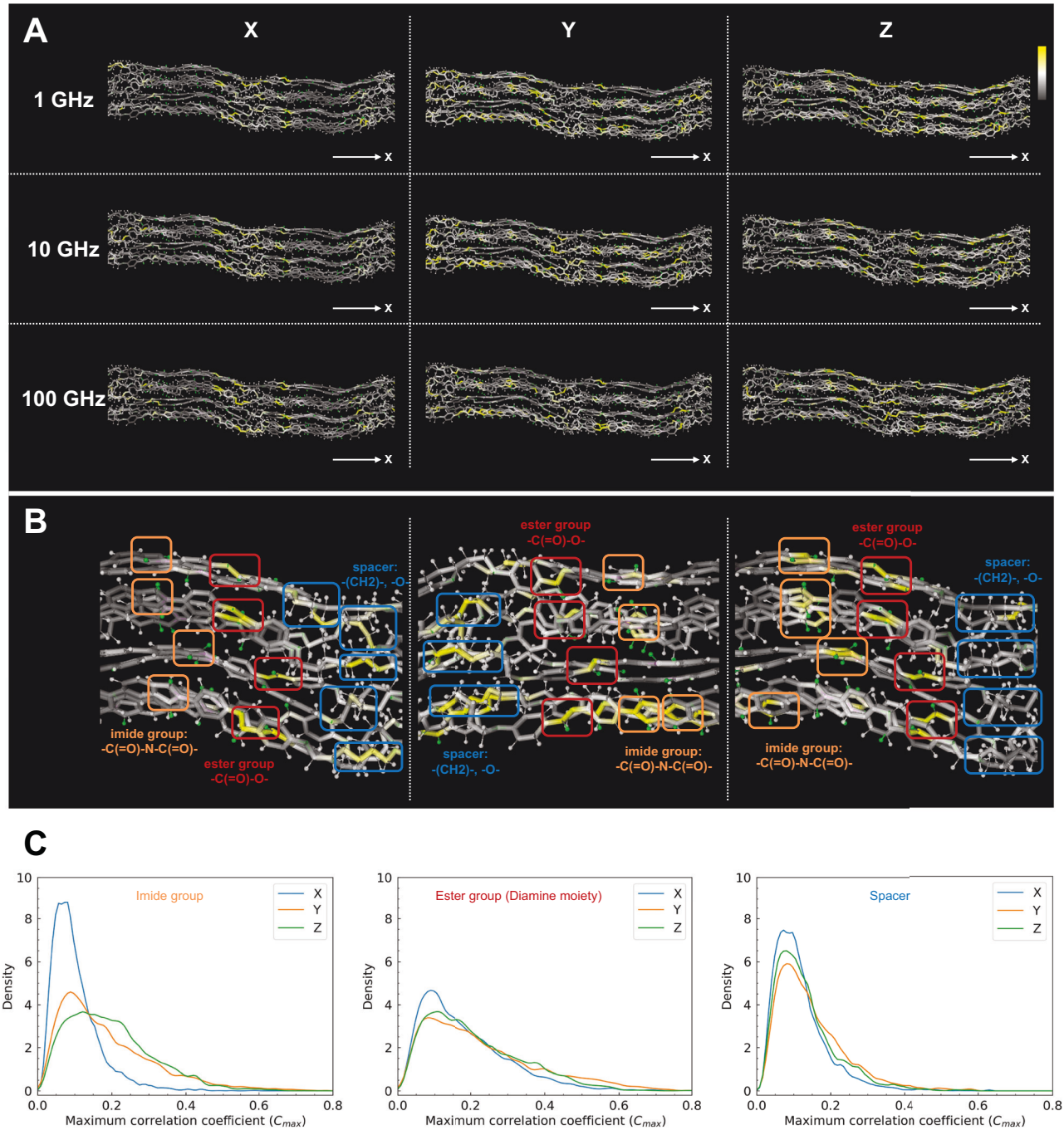

Fig. 5 Visualization of the cross-correlation coefficient $C_{\max}$ for each segment along the polymer chain in PI-B6, showing the periodic torsional motion induced by the applied electric field across different polymer chain segments at various frequencies. As the $C_{\max}$ values increase, the color transitions from black to white to yellow, indicating regions within the PI chains where periodic motion occurs. **A** Results for $C_{\max}$ at 1 GHz, 10 GHz, and 100 GHz when a virtual alternating electric field is applied in the X, Y, and Z directions (with the X direction aligned along the molecular chain orientation). **B** Enlarged view of the 10 GHz results with key functional groups highlighted by colored rectangles. **C** Probability density distributions of $C_{\max}$ for the imide, ester, and spacer parts

polymeric materials for high-frequency applications but also a framework for developing advanced PI materials tailored to high-frequency wireless communication applications.

Data availability

The data that support the findings of this study are available from the corresponding author upon reasonable request.

Acknowledgements The synchrotron radiation experiments were performed at the BL40B2 of SPring-8 with the approval of the Japan Synchrotron Radiation Research Institute (JASRI) (Proposal No. 2022B1131), with support from Dr. Noboru Ohta (JASRI) and Prof. Tomoyasu Hirai (Osaka Institute of Technology). Some of the simulations were performed via Fugaku at the RIKEN Center for Computational Science, Kobe, Japan, and the supercomputer at the Research Center for Computational Science, Okazaki, Japan (Project: 23-IMS-C099, 24-IMS-C09). This work was supported by the Japan Science and Technology Agency (JST) under the CREST program (Grant Number JPMJCR19I3) (JM, TH), the Japan Society for the Promotion of Science (JSPS) through the KAKENHI program (Grant Number 21K04828) (YN), and the Ministry of Education, Culture, Sports, Science and Technology through the "Program for Promoting Research on the Supercomputer Fugaku" (Project ID: hp210264) (RY). HM and RM were supported by JST SPRING (Grant Numbers JPMJSP2106 and JPMJSP2180).

Compliance with ethical standards

Conflict of interest The authors declare no competing interests.

References

1. Volksen W, Miller RD, Dubois G. Low dielectric constant materials. Chem Rev. 2010;110:56–110.
2. Maier G. Low dielectric constant polymers for microelectronics. Prog Polym Sci. 2001;26:3–65.
3. Zhao X, Liu H. Review of polymer materials with low dielectric constant. Polym Int. 2010;59:597–606.
4. Tang L, Zhang J, Tang Y, Kong J, Liu T, Gu J. Polymer matrix wave-transparent composites: a review. J Mater Sci Technol. 2021;75:225–51.
5. Wang L, Yang J, Cheng W, Zou J, Zhao D. Progress on polymer composites with low dielectric constant and low dielectric loss for high-frequency signal transmission. Front Mater. 2021;8:774843.
6. Li Y, Sun G, Zhou Y, Liu G, Wang J, Han S. Progress in low dielectric polyimide film – a review. Prog Org Coat. 2022;172:107103.
7. Liaw D-J, Wang K-L, Huang Y-C, Lee K-R, Lai J-Y, Ha C-S. Advanced polyimide materials: syntheses, physical properties and applications. Prog Polym Sci. 2012;37:907–74.
8. Zhang C, He X, Lu Q. High-frequency low-dielectric-loss in linear-backbone-structured polyimides with ester groups and ether bonds. Commun Mater. 2024:5.
9. Mi M-C, Szu F-E, Cheng Y-C, Tsai C-H, Chen J-H, Huang J-H, et al. Semiaromatic poly(ester imide) copolymers with alicyclic diamines for low-k properties at a high frequency of 10–40 GHz. ACS Appl Polym Mater. 2024;6:11137–48.
10. Yin Q, Qin Y, Lv J, Wang X, Luo L, Liu X. Reducing intermolecular friction work: preparation of polyimide films with ultralow dielectric loss from MHz to THz frequency. Ind Eng Chem Res. 2022;61:17894–903.
11. Kuo CC, Lin YC, Chen YC, Wu PH, Ando S, Ueda M, et al. Correlating the molecular structure of polyimides with the dielectric constant and dissipation factor at a high frequency of 10 GHz. ACS Appl Polym Mater. 2021;3:362–71.
12. Sawada R, Ando S. Colorless, low dielectric, and optically active semialicyclic polyimides incorporating a biobased isosorbide moiety in the main chain. Macromolecules. 2022;55:6787–6800.
13. Sawada R, Ando S. Polarization analysis and humidity dependence of dielectric properties of aromatic and semialicyclic polyimides measured at 10 GHz. J Phys Chem C. 2024;128:6979–90.
14. Liu Y, Zhao X-Y, Sun Y-G, Li W-Z, Zhang X-S, Luan J. Synthesis and applications of low dielectric polyimide. Resour Chem Mater. 2023;2:49–62.
15. Nagella SR, Ha C-S. Structural designs of transparent polyimide films with low dielectric properties and low water absorption: a review. Nanomaterials. 2023;13:2090.
16. Zhang D, Li L, Wang Y, Zhang C, Teng C. Methods and strategies to decrease the dielectric properties of polyimide films: a review. J Solgel Sci Technol. 2023;108:1–12.
17. Simpson JO, St.Clair AK. Fundamental insight on developing low dielectric constant polyimides. Thin Solid Films. 1997;308–309:480–5.
18. Ahmad Z. in Dielectric material. InTech; 2012. https://doi.org/10.5772/50638.
19. Van Krevelen DW, Te Nijenhuis K. Polymer properties. In: Properties of polymers. 2009. pp. 3–5. https://doi.org/10.1016/B978-0-08-054819-7.00001-7.
20. Goto K, Akiike T, Inoue Y, Matsubara M. Polymer design for thermally stable polyimides with low dielectric constant. Macromol. Symp. 2003;199:321–32.
21. Tao L, Yang H, Liu J, Fan L, Yang S. Synthesis and characterization of highly optical transparent and low dielectric constant fluorinated polyimides. Polymer. 2009;50:6009–18.
22. He J, Wu X, Cheng Y. Low dielectric post-cured benzocyclobutene-functionalized fluorine-containing polyimide material. Eur Polym J. 2023;196:112334.
23. Baek Y, Lim S, Yoo EJ, Kim LH, Kim H, Lee SW, et al. Fluorinated polyimide gate dielectrics for the advancing the electrical stability of organic field-effect transistors. ACS Appl Mater Interfaces. 2014;6:15209–16.
24. Watanabe Y, Shibasaki Y, Ando S, Ueda M. Synthesis of semiaromatic polyimides from aromatic diamines containing adamantyl units and alicyclic dianhydrides. J Polym Sci A Polym Chem. 2004;42:144–50.
25. Watanabe Y, Shibasaki Y, Ando S, Ueda M. New negative-type photosensitive alkaline-developable semi-aromatic polyimides with low dielectric constants based on poly(amic acid) from aromatic diamine containing adamantyl units and alicyclic dianhydrides, a cross-linker, and a photoacid generator. Polym J. 2005;37:270–6.
26. Watanabe Y, Sakai Y, Shibasaki Y, Ando S, Ueda M, Oishi Y, et al. Synthesis of wholly alicyclic polyimides from N-silylated alicyclic diamines and alicyclic dianhydrides. Macromolecules. 2002;35:2277–81.
27. Chern YT, Tsai JY. Low dielectric constant and high organosolubility of novel polyimide derived from unsymmetric 1,4-Bis(4-aminophenoxy)-2,6-di-tert-butylbenzene. Macromolecules. 2008;41:9556–64.
28. Wu S, Hayakawa T, Kikuchi R, Grunzinger SJ, Kakimoto MA, Oikawa H. Synthesis and characterization of semiaromatic polyimides

containing POSS in main chain derived from double-decker-shaped silsesquioxane. Macromolecules. 2007;40:5698–705.
29. Wu S, Hayakawa T, Kakimoto MA, Oikawa H. Synthesis and characterization of organosoluble aromatic polyimides containing POSS in main chain derived from double-decker-shaped silsesquioxane. Macromolecules. 2008;41:3481–7.
30. Han J, Kiss L, Mei H, Remete AM, Ponikvar-Svet M, Sedgwick DM, et al. Chemical aspects of human and environmental overload with fluorine. Chem Rev. 2021:121:4678–742.
31. Lohmann R, Cousins IT, DeWitt JC, Glüge J, Goldenman G, Herzke D, et al. Are fluoropolymers really of low concern for human and environmental health and separate from other PFAS? Environ Sci Technol. 2020;54:12820–8.
32. Araki H, Kiuchi Y, Shimada A, Ogasawara H, Jukei M, Tomikawa M. Low Df polyimide with photosensitivity for high frequency applications. J. Photopolym. Sci. Technol. 2020;33:165–170.
33. Minakov, AA, Schick, C Ultrafast thermal processing and nanocalorimetry at heating and cooling rates up to 1MK⁄s. Rev. Sci. Instrum. 2007;78:073902.
34. Thompson AP, Aktulga HM, Berger R, Bolintineanu DS, Brown WM, Crozier PS, et al. LAMMPS - a flexible simulation tool for particle-based materials modeling at the atomic, meso, and continuum scales. Comput Phys Commun. 2022;271:108171.
35. Hayashi Y, Shiomi J, Morikawa J, Yoshida R. RadonPy: automated physical property calculation using all-atom classical molecular dynamics simulations for polymer informatics. NPJ Comput Mater. 2022;8:222.
36. Winmostar V9, X-Ability Co. Ltd., Tokyo, Japan; 2019.
37. Träg J, Zahn D. Improved GAFF2 parameters for fluorinated alkanes and mixed hydro- and fluorocarbons. J Mol Model. 2019;25:39.
38. Collings PJ, Hird M. Introduction to liquid crystals chemistry and physics. CRC Press; 2017.
39. Donald AM, Windle AH, Hanna S. Liquid crystalline polymers. Cambridge University Press; 2006.
40. Wang X-J, Zhou Q-F. Liquid crystalline polymers. World Scientific; 2004. https://doi.org/10.1142/5309.
41. Ober CK, Jin J-I, Zhou Q, Lenz, RW. in 1984. pp. 103–46. https://doi.org/10.1007/3-540-12818-2_8.
42. Wunderlich B, Grebowicz, J. in 1984. pp. 1–59. https://doi.org/10.1007/3-540-12994-4_1.
43. Lee K-W, Su S-H, Hsiang S-J, Lin C-H, Hsiao W-L, Yeh R-Y. Diamine monomer compound and its preparing method, resin, flexible film, and electronic device. US Patent 20230086746 A1, 2023.
44. Kricheldorf HR, Linzer V. Liquid crystalline polyimides: 18. Thermotropic polyimides based on biphenyl-3,3',4,4'-tetracarboxylic anhydride. Polymer. 1995;36:1893–1902.
45. Maeda H, Wu S, Marui R, Yoshida E, Hatakeyama-Sato K, Nabae Y, et al. Discovery of liquid crystalline polymers with high thermal conductivity using machine learning. ChemRxiv. [Preprint]. 2024. Available from: https://doi.org/10.26434/chemrxiv-2024-tj786.
46. Bei R, Chen K, He Y, Li C, Chi Z, Liu S, et al. A systematic study of the relationship between the high-frequency dielectric dissipation factor and water adsorption of polyimide films. J Mater Chem C Mater. 2023;11:10274–81.
47. Bei R, Chen K, Liu Q, He Y, Li C, Huang H, et al. Relationship among the water adsorption, polymer structure, and high-frequency dissipation factor: precise analysis of water adsorption of low-dielectric constant polyimide films. Macromolecules. 2024;57:2142–53.
48. Osaki S, Tashiro K. Molecular orientation and dielectric anisotropy in polyimide films as determined by the microwave method. Macromolecules. 1998;31:1661–64.